

Search of keV Sterile Neutrino Warm Dark Matter in the Rhenium and Tritium beta decays

H.J. de Vega

*LPTHE Université Pierre et Marie Curie (Paris VI) et Denis Diderot (Paris VII),
Laboratoire Associé au CNRS UMR 7589, Tour 24, 5eme. étage,
Boite 126, Place Jussieu, 75252 Paris, Cedex 05, France*

O. Moreno and E. Moya de Guerra

*Departamento de Física Atómica, Molecular y Nuclear,
Facultad de Ciencias Físicas, Universidad Complutense, 28040 Madrid, Spain*

M. Ramón Medrano

Departamento de Física Teórica I, Facultad de Ciencias Físicas, Universidad Complutense, 28040 Madrid, Spain

N. G. Sánchez

Observatoire de Paris, LERMA. Laboratoire Associé au CNRS UMR 8112

(Dated: December 3, 2024)

keV sterile neutrinos are important as extensions of the Standard Model of particle physics and as serious keV dark matter (DM) candidates (Warm DM) in agreement with both cosmological and galaxy observations. We study the possible detection of a keV sterile neutrino through its mixing with a light active neutrino in the Rhenium 187 and Tritium beta decays. The electron *low* energy beta spectrum $0 \text{ keV} \lesssim T_e \lesssim (Q_\beta - m_s) \text{ keV}$ is the region where a sterile neutrino could be detected and its mass m_s measured, (m_s being expected 1 to 10 keV from cosmological and galactic observations and theoretical analysis). This region is away from the near end-point Q_β region suitable to measure the mass of the light active neutrino. In order to analyze the sterile neutrino effect, we introduce the dimensionless ratio \mathcal{R} of the sterile neutrino to the active neutrino contribution: \mathcal{R} exhibits a constant plateau that starts at momentum $p_e = 0$ and sharply drops for p_e near its maximum value; \mathcal{R} increases with the mixing angle and decreases for increasing sterile neutrino mass m_s . The Kurie function is expressed in terms of \mathcal{R} and reflects its properties. For ^{187}Re the p-wave electrons dominate the decay by a factor 10^4 over the s-wave electrons while the Tritium decays exclusively through the s-wave electrons. Two very important experiments are running at present: MARE and KATRIN for Rhenium 187 and Tritium beta decays respectively; (KATRIN concentrates on the end-point electron region but if appropriately modified could look for the keV sterile neutrino as well). The carefully computed decay rates and spectra support that the largest realistic ratio \mathcal{R} is about 10^{-8} for current sterile neutrino models, and the sterile neutrino probability [for typical 10 years of MARE data acquisition] is about $10^5 - 10^7$, which is not negligible, [namely, $10^5 - 10^7$ sterile neutrinos in $10^{13} - 10^{15}$ events]. A more precise detection probability should include a careful analysis of the systematic errors, which is beyond the scope of this paper.

PACS numbers: 23.40.-s, 14.60.St, 14.60.Pq, 95.35.+d

Keywords: keV sterile neutrinos, beta decay, warm dark matter

Contents

I. Introduction	2
II. Dark matter	3
III. Dark matter and keV sterile neutrinos	4
IV. The sterile neutrino mass and the Rhenium 187 beta decay	5
A. The ratio of the sterile neutrino to the active neutrino contribution and the Kurie plot	8
V. The sterile neutrino mass and the Tritium beta decay	12
VI. Conclusions	14

I. INTRODUCTION

It is well known that dark matter (DM) is not described by the Standard Model (SM) of particle physics. Many extensions can be envisaged to include DM particles, coupled weakly enough to the SM particles to fulfill all particle experimental constraints, namely the fact that DM has not been detected so far in any particle physics experiment. On the other hand, cosmological and astrophysical constraints such as the ones coming from the dark matter density and the galaxy phase space density, or alternatively, the universal galaxy surface density, lead to DM candidates in the keV mass scale, namely Warm DM (WDM), refs. [1–5]. A keV mass scale sterile neutrino is the front running candidate for WDM. Other WDM candidates in the keV mass scale are: gravitinos, light neutralino and majorons [1, 6].

Considering the first WDM candidate, sterile neutrinos can be naturally embedded in the SM of particle physics. They do not participate in weak interactions, and hence they are singlets of color, weak SU(2) and weak hypercharge. One sterile neutrino per lepton family is expected, but only the lightest one (i.e. electron family) has a life time of the order of Hubble time and can describe the DM.

In this work, we consider Rhenium 187 and Tritium beta decay experiments to detect a keV mass sterile neutrino as a DM candidate. The left neutrino flavor state ν_e (and equivalently for $\bar{\nu}_e$) will be a mixing of two mass eigenstates: one light active neutrino mass state (ν_l) and one keV scale sterile neutrino mass state (ν_s). Other neutrino mass states will not be taken into account for the time being. The mass m_l of the lightest active neutrino state is negligible ($m_l \ll \text{eV}$) in comparison with the mass m_s of the keV sterile mass state. The smallness of the mixing angle ζ makes sterile neutrinos difficult to detect.

Sterile neutrinos in the beta decay of Rhenium 187 are currently searched by the Microcalorimeter Arrays for a Rhenium Experiment (MARE) [7]. In this decay the available energy is $Q_\beta(^{187}\text{Re}) \simeq 2.47$ keV. The beta decay of Rhenium 187 into Osmium 187 is a first forbidden unique Gamow-Teller process ($5/2^+ \rightarrow 1/2^-$).

Up to now, the no observation of keV scale sterile neutrinos in the beta decay of Rhenium 187 gave an upper bound on the mixing angle $\zeta < 0.095$ for 1 keV steriles [8], which is compatible with the cosmological constraints on the mixing angle, $\zeta \sim 10^{-4}$, appropriate to produce enough sterile neutrinos to account for the observed DM. However, the amount of the sterile neutrinos that could be produced in the early universe also depends on the production mechanism which is model dependent.

The Karlsruhe Tritium Neutrino Experiment (KATRIN) is currently studying the Tritium beta decay [11] and, if suitably adapted, it could show the presence of a sterile neutrino as well. In this decay the available energy is $Q_\beta(^3\text{H}_1) \simeq 18.6$ keV. The beta decay of Tritium into Helium 3 is an allowed transition ($1/2^+ \rightarrow 1/2^+$) with Fermi and Gamow-Teller contributions. Clearly, KATRIN has the potential to detect sterile neutrinos with mass up to 18 keV.

In Sections II and III we deal with keV dark matter from the cosmological and galactic point of view. WDM (DM particle mass between 1 keV and 10 keV, and decoupling temperature $T_d \sim 100$ GeV) produces the observed small (galactic) structures, as well as the large scale and cosmological structures, the observed cored density profiles and the right surface density value, while GeV WIMPS ($m \sim 100$ GeV, and $T_d \sim 5$ GeV, Cold DM) inevitably produce a host of non observed small scale structures, non observed cusped profiles and values of the galaxy surface density much higher than the observed value.

In Section IV we analyze the possible detection of a sterile neutrino in the Rhenium beta decay. Contributions for the electron *s*- and *p*-waves have to be taken into account [9, 10]. For the detection of a sterile neutrino, the important electron kinetic energy range T_e is between 0 and $(Q_\beta - m_s)$, m_s being the mass of the keV sterile neutrino. On the contrary, the electron kinetic energy region close to the end-point energy Q_β is the one suitable for the detection of light active neutrinos. Systematic uncertainties such as Beta Environmental Fine Structure (BEFS) are not considered here [7]. In order to analyze the sterile neutrino effect, we introduce the dimensionless ratio \mathcal{R} of the sterile neutrino to the active neutrino contribution: \mathcal{R} is largest for T_e (or the electronic momentum p_e) going to zero. This procedure is useful because it allows us to compare two regions of the same spectrum: the one where the keV neutrino imprints a glitch on the spectrum and the opposite side (near the end-point) where the active light neutrino effect shows up. For ^{187}Re the electrons emitted in the *p*-wave dominate the decay by a factor 10^4 over the *s*-wave. \mathcal{R} is non-zero in a

range $0 \leq p_e < (p_e)_{\max}$, the maximum momentum $(p_e)_{\max}$ decreases with increasing mass m_s . \mathcal{R} exhibits a constant plateau that starts at $p_e = 0$ and sharply drops for p_e near $(p_e)_{\max}$.

\mathcal{R} increases with the mixing angle and decreases for increasing mass m_s . The Kurie function is expressed in terms of \mathcal{R} and the above properties reflect themselves in the obtained Kurie plots.

In Section V we study the possible detection of a sterile neutrino in the Tritium decay [11]. Here, only the electron s -wave contributes. Analogously to the Rhenium beta decay, the important kinetic energy region for the sterile neutrino detection is the low energy range $0 \leq T_e \leq (Q_\beta - m_s)$ while for active neutrinos it is the one close to the end-point energy Q_β . The properties of the ratio \mathcal{R} and Kurie functions are similar to those obtained in the Rhenium case.

In Section VI we present our conclusions. The low electron energy domain of the beta spectrum is the region where a sterile neutrino could be detected and its mass measured, the expected mass being in the keV scale (1 to 10 keV) as constrained from cosmological and galactic observations and theoretical analysis. We found that the largest ratio \mathcal{R} for a realistic mixing angle is about 10^{-8} , [dotted line and small p_e region in Fig. 5]. In order to detect such a small sterile neutrino effect, the number of detected events N_β must be increased, (for instance by choosing a small Q_β value, as it is the case of the Rhenium, and by increasing the time of data acquisition). We evaluate the sterile neutrino probability $\mathcal{R} \times N_\beta$ is about $10^5 - 10^6$, which is not negligible; (for a MARE number of events of $10^{13} - 10^{14}$, 10 years of data acquisition, 8 arrays and 400 gr of natural Rhenium [7]). That means to find such $10^5 - 10^6$ sterile neutrinos in those $10^{13} - 10^{14}$ events. This probability is increased to 10^7 for the MARE option of 10^{15} events, (10 years of data acquisition, 16 arrays and 3.2 kg of natural Rhenium, [7]). Of course, in order to assess a precise detection probability one should include a careful analysis of the systematic errors and instrument parameters, but such study is beyond the scope of the present paper. Natural units $\hbar = c = 1$ are used all over this paper.

II. DARK MATTER

Although dark matter was noticed seventy-five years ago [12, 13] its nature is not yet known. Dark matter (DM) is needed to explain the observed structures in the Universe, in particular galaxies. DM particles must be non-relativistic by the time of structure formation in order to reproduce the observed small structure at $\sim 2 - 3$ kpc.

The connection between the scale of the formed structure and the mass of the DM particle follows from the value of the free-streaming length l_{fs} [14]. This is the distance that the DM particles can freely travel. Structures at scales smaller than l_{fs} are erased by free-streaming and hence l_{fs} provides a lower bound on the size of DM dominated structures. WDM particles with mass in the keV scale give $l_{fs} \sim 100$ kpc while 100 GeV cold dark matter (CDM) particles produce an extremely small $l_{fs} \sim 0.1$ pc. A $l_{fs} \sim 100$ kpc is in nice agreement with the astronomical observations on galaxies [15] (smaller objects like stars are formed by baryons, not by DM), as well as on cosmological scales.

The GeV CDM l_{fs} is a million times smaller and would lead to the existence of a host of CDM smaller scale structures till the size of the solar system. No structures of such type have ever been observed. Lighter DM particles in the eV scale (hot dark matter, HDM) have a free-streaming length $l_{fs} \sim \text{Mpc}$ and hence would erase all existing structures below the Mpc scale in contradiction with all observations. This is why HDM cannot be considered [16].

The reason why CDM does not work is simple: CDM particles in the GeV scale are too slow (too cold) which prevent them to erase the small scale structure, while the eV particles (HDM) are excessively fast, which erase all structures; in between, WDM keV particles are able to produce the observed structures.

Astronomical observations strongly indicate that dark matter halos have cored profiles till scales below 1 kpc. On the contrary, CDM simulations (particles heavier than 1 GeV) always give cusped profiles. No cusped profiles have been ever observed. Linear profiles computed from the Boltzmann-Vlasov equation turn out to be cored for WDM and cusped for CDM indicating that WDM does reproduce the astronomical observations [4].

The surface density in DM dominated galaxies is defined by $\mu_0 \equiv \rho_0 r_0$ where ρ_0 is the central core density and r_0 is the core radius for DM dominated galaxies. μ_0 turns out to be universal, taking the same value up to $\pm 10\%$ for galaxies of different sizes, morphologies, Hubble types and luminosities [17]. The surface density value predicted by CDM simulations is 1000 times larger than the observed value [18], while the surface density for keV WDM computed from the Boltzmann-Vlasov equation is in full agreement with the observed value of $120 (\text{MeV})^3$ indicating again that WDM does reproduce the astronomical observations [4].

Combining theoretical analysis with the observed values of the dark matter density and the phase space density today (density over the cube of the velocity dispersion) of dwarf spheroidal galaxies constrains the mass to be in the $\sim \text{keV}$ range [3].

Recent radioastronomy observations of velocity widths in galaxies from 21cm HI surveys clearly favours WDM over CDM [19]. WDM simulations contrasted to astronomical observations suggest a WDM particle mass slightly above 1 keV. Constraints from large scale structure give this value too [20]. Recent cosmological WDM N-body simulations with keV sterile neutrino WDM clearly show the agreement of the predicted small scale structures with the observations, while CDM simulations do not agree with observations at such scales [21].

None of the predictions of CDM simulations at small scales (cusps, substructures, dark disks, ...) have been observed. For example, the CDM satellite problem (CDM simulations predict too many satellites in the Milky Way; only 1/3 of satellites predicted by CDM simulations around our galaxy are observed) ; the surface density problem (the galaxy surface density value for CDM simulations is 1000 larger than observed [4, 18]); the voids problem and the size problem (CDM simulations do not produce big enough galaxies) [22–24].

Notice that all DM observable effects discussed above only arise from the gravitational behaviour of the DM. Galaxy properties are independent of the spin, statistics and non-gravitational couplings of the DM particles, provided that their couplings are small enough.

DM may decouple at or out of thermal equilibrium. The distribution function freezes out at decoupling. Whether they decouple at or out of equilibrium depends on the non-gravitational couplings of the DM particle. Normally, sterile neutrinos are so weakly coupled that they decouple out of thermal equilibrium. The functional form of the DM distribution function depends on the DM particle couplings and is therefore model dependent.

Sterile neutrinos can decay into an active-like neutrino and a monochromatic X-ray photon with an energy half the mass of the sterile neutrino. Observing the X-ray photon provides a way to observe sterile neutrinos in DM halos [25].

WDM keV sterile neutrinos can be copiously produced in the supernovae cores. Supernovae (SN) stringently constrain the neutrino mixing angle squared to be $\lesssim 10^{-9}$ for $m > 100$ keV (in order to avoid excessive energy lost) but for smaller masses the SN bound is not so direct. Within the models worked out till now, mixing angles are essentially unconstrained by SN in the keV mass range [26].

Sterile neutrinos are produced out of thermal equilibrium and their production can be non-resonant (in the absence of lepton asymmetries) or resonantly enhanced (if lepton asymmetries are present). keV sterile neutrino WDM in minimal extensions of the Standard Model is consistent with Lyman-alpha constraints within a wide range of the model parameters. Lyman-alpha observations give a lower bound for the sterile neutrino mass of 4 keV only for sterile neutrinos produced in the case of a non-resonant (Dodelson-Widrow) mechanism [27, 28]. The Lyman-alpha lower bounds for the WDM particle mass are smaller in the Neutrino Minimal Standard Model (sterile neutrinos produced by the decay of a heavy neutral scalar) and for fermions in thermal equilibrium.

Moreover, the number of observed Milky-Way satellites indicates lower bounds between 2 and 13 keV for different models of sterile neutrinos.

In summary, contrary to CDM, WDM essentially *works*, naturally reproducing the astronomical observations of structures over all scales, small as well as large and cosmological scales. The sterile neutrino with mass in the keV scale appears as a serious candidate for WDM. Galaxy observations alone cannot determine the DM particle properties other than the mass and the decoupling temperature. A direct particle detection is necessary to pinpoint and determine which particle candidate describes the dark matter. Beta decay is a promising way to detect DM sterile neutrinos.

III. DARK MATTER AND KEV STERILE NEUTRINOS

As is known, DM is not described by the Standard Model of particle physics (SM). Many extensions of the SM can be envisaged to include a DM particle with mass in the keV scale and coupled weakly enough to the Standard Model particles to fulfill all particle physics experimental constraints, namely, the fact that the DM has not been detected so far in any particle physics experiment.

Besides sterile neutrinos, possible DM candidates in the keV mass scale are: gravitinos, light neutralino, majoron [6].

As particle physics motivations for sterile neutrinos one can advance that there are both left and right handed quarks (with respect to the chirality) while active neutrinos are only left handed. It is thus natural to have right handed neutrinos ν_R besides the known left-handed active neutrino. This argument is the so-called ‘quark-lepton similarity’.

Sterile neutrinos can be naturally embedded in the SM of particle physics with the symmetry group $SU(3)_{color} \otimes SU(2)_{weak} \otimes U(1)_{weak\ hypercharge}$.

Leptons are color singlets and doublets under weak SU(2) in the SM. Sterile neutrinos ν_R do not participate to weak interactions. Hence, they must be **singlets** of color, weak SU(2) and weak hypercharge.

Let us consider a simple embedding of the sterile neutrino in the Standard Model. More elaborated sterile neutrino models have been put forward [31].

The SM Higgs Φ is a $SU(2)$ doublet with a nonzero vacuum expectation value Φ_0 . This allows a Yukawa-type coupling with the left and right handed leptons:

$$L_{Yuk} = y \bar{\nu}_L \nu_R \Phi_0 + h.c. \quad , \quad (1)$$

where y = Yukawa coupling,

$$\Phi_0 = \begin{pmatrix} 0 \\ v \end{pmatrix} \quad , \quad v = 174 \text{ GeV} .$$

These terms in the Lagrangian induce a mixing (bilinear) term between ν_L and ν_R which produces transmutations $\nu_L \Leftrightarrow \nu_R$. Mixing and oscillations of particle states are typical of low energy particle physics. Further well known examples are: (i) flavor mixing: e - μ neutrino oscillations (explain solar neutrinos), (ii) $K^0 - \bar{K}^0$, $B^0 - \bar{B}^0$ and $D^0 - \bar{D}^0$ meson oscillations in connection with CP-violation.

As a consequence of the Lagrangian eq.(1), the neutrino mass matrix takes the form:

$$(\bar{\nu}_L \ \bar{\nu}_R) \begin{pmatrix} 0 & m_D \\ m_D & M \end{pmatrix} \begin{pmatrix} \nu_L \\ \nu_R \end{pmatrix}$$

where M is the mass term of the right-handed neutrino ν_R , $m_D = y v$ and $M \gg m_D$.

The masses of the active and sterile neutrinos are given by the seesaw mechanism. The mass eigenvalues in this simple model take the form: m_D^2/M (active neutrino) and M (sterile neutrino), with eigenvectors:

- active neutrino: $\nu_{active} \simeq \nu_L - \frac{m_D}{M} \nu_R$.
- sterile neutrino: $\nu_{sterile} \simeq \nu_R + \frac{m_D}{M} \nu_L$, $M \gg m_D^2/M$.

Choosing $M \sim 1$ keV and $m_D \sim 0.1$ eV yields m_D^2/M about 10^{-5} eV consistent with observations. This corresponds to a mixing angle $\zeta \sim m_D/M$ about 10^{-4} and would be appropriate to produce enough sterile neutrinos accounting for the observed DM. However, notice that the amount of the sterile neutrinos produced in the early universe also depends on the production mechanism which is model dependent. The smallness of the mixing angle ζ makes sterile neutrinos difficult to detect.

Sterile neutrinos in the beta decay of Rhenium 187 are currently searched for by the MARE experiment [7]: $^{187}\text{Re} \rightarrow ^{187}\text{Os} + e^- + \bar{\nu}_e$. In this decay the available energy: is $Q(^{187}\text{Re}) \simeq 2.47$ keV. Up to now, the no observation of keV sterile neutrinos in the Rhenium 187 beta decay gave the upper bound $\zeta < 0.095$ for 1 keV sterile neutrinos [8]. This value is largely compatible with the cosmological constraints on the mixing angle.

On the other hand, precise measurements of nucleus recoil in Tritium beta decay: $^3\text{H}_1 \rightarrow ^3\text{He}_2 + e^- + \bar{\nu}$ can show the presence of a sterile neutrino instead of an ordinary active $\bar{\nu}$ in the decay products. In this decay the end-point energy is $Q(^3\text{H}_1) \simeq 18.6$ keV. The KATRIN experiment is currently studying this beta decay in the end-point region [11].

Concerning the number of sterile neutrinos, one sterile neutrino per lepton family is expected. Only the lightest one (ie. electron family) has a lifetime \sim Hubble time and can describe the DM.

In summary, the empty slot of right-handed neutrinos in the Standard Model of particle physics can be filled, in a fully consistent way, by keV-scale sterile neutrinos describing the DM.

IV. THE STERILE NEUTRINO MASS AND THE RHENIUM 187 BETA DECAY

As a probe to detect possible mixing of keV sterile neutrinos with light active neutrinos, we consider the beta decay of Rhenium 187 (^{187}Re ; $Z = 75$, $A = 187$) into Osmium 187 (^{187}Os ; $Z = 76$, $A = 187$),

$$^{187}\text{Re} \rightarrow ^{187}\text{Os} + e^- + \bar{\nu}_e \quad (2)$$

The neutrino flavor eigenstate ν_e (and equivalently for $\bar{\nu}_e$) can be written as a combination of mass eigenstates of light active (subscript i) and heavier mass states.

$$|\nu_e\rangle = \sum_i U_{ei} |\nu_i\rangle + \sum_s U_{es} |\nu_s\rangle \quad (3)$$

where the quantities U belong to the unitary leptonic mixing matrix. For the purpose of this paper, we approximate this combination as a two mass-eigenstate mixing given by

$$|\nu_e\rangle = \cos \zeta |\nu_l\rangle + \sin \zeta |\nu_s\rangle \quad (4)$$

where ζ is the mixing angle between a light neutrino mass state ν_l , and the heavy sterile neutrino mass state ν_s . Other neutrino mass states will not be taken into account for the time being.

An effective mass m_l can be used for the former combination of light mass active neutrinos, but its value ($m_l \lesssim$ eV) is negligible in comparison with the sterile neutrino mass in the keV scale.

As for the mixing angle ζ , the cosmological constraints based on the observed average DM density suggest [5]

$$\sin^2 \zeta \sim 10^{-8} \quad , \quad \zeta \sim 0.006^\circ \quad . \quad (5)$$

However, these constraints on the value of ζ depend both on the sterile neutrino model and on the sterile neutrino production mechanism. Eq.(5) corresponds to currently popular models of DM sterile neutrino [5].

^{187}Re is a long half-life isotope ($t_{1/2} \simeq 4.35 \cdot 10^{10}$ years), with ground state spin-parity assignment $J^\pi = 5/2^+$, that has a single β^- -decay branch mode to the ground state $1/2^-$ of ^{187}Os , with an endpoint energy $Q_\beta \simeq 2.47$ keV ($Q_\beta = T_e + m_\nu + T_\nu$).

In this transition, the change in total angular momentum is $\Delta J = 2$ and there is also a change of parity ($\Delta\pi = -$), therefore we are dealing at best with a first forbidden Gamow-Teller process. The lepton system ($e - \bar{\nu}$) carries an orbital angular momentum $L = 1$ (first forbidden transition) and a spin $S = 1$ (unique Gamow-Teller transition), that couple to the total angular momentum $J = 2$. The two possible angular components of the system, $[(l_j)_e(l_j)_{\bar{\nu}}]_{J=2}$, are $[(p_{3/2})_e(s_{1/2})_{\bar{\nu}}]_{J=2}$ and $[(s_{1/2})_e(p_{3/2})_{\bar{\nu}}]_{J=2}$. Therefore, as noted in [9], the total differential decay rate $d\Gamma/dE_e$ is a sum of the two contributions corresponding to the emission of electrons in p -wave and s -wave

$$\frac{d\Gamma}{dE_e} = \frac{d\Gamma_{p_{3/2}}}{dE_e} + \frac{d\Gamma_{s_{1/2}}}{dE_e} \quad (6)$$

Following eq. (4), we write the theoretical spectral shape of the electron in an (l_j) -wave as a sum of the contributions from active (light, l) and sterile (s) neutrinos,

$$\frac{d\Gamma_{l_j}}{dE_e} = \frac{d\Gamma_{l_j}^l}{dE_e} \cos^2 \zeta + \frac{d\Gamma_{l_j}^s}{dE_e} \sin^2 \zeta \quad (7)$$

where

$$\frac{d\Gamma_{l_j}^\chi}{dE_e} = C B_{Re} R_{Re}^2 p_e p_{\nu_\chi} E_e (E_0 - E_e) F_0(Z, E_e) S_l(p_e, p_{\nu_\chi}) \theta(E_0 - E_e - m_\chi) , \quad (8)$$

for $\chi = l, s$; Z stands for the atomic number of the daughter nucleus, $F_0(Z, E_e)$ is the Fermi function and $\theta(E_0 - E_e - m_\chi)$ is the step function; B_{Re} is the dimensionless squared nuclear reduced matrix element (r.m.e), and C is a constant, both to be defined later on; R_{Re} is the nuclear radius [32]. In the above expression, E_e , E_0 and $p_e = \sqrt{E_e^2 - m_e^2}$ are the total energy, maximum total energy and momentum of the emitted electron respectively, and $p_\nu = \sqrt{(E_0 - E_e)^2 + m_\nu^2}$ is the momentum of the emitted neutrino.

Being Q_β the end-point energy, we have $E_0 = m_e + Q_\beta$ for zero neutrino mass, and the kinematical ranges of E_e , p_e and p_ν are:

$$m_e \leq E_e \leq m_e + Q_\beta; \quad 0 \leq p_e \leq \sqrt{Q_\beta^2 + 2m_e Q_\beta}; \quad 0 \leq p_\nu \leq Q_\beta. \quad (9)$$

The shape factor $S_l(p_e, p_\nu)$ appears in forbidden decays and for the case of interest here, a first forbidden decay, l takes the value $l = 0$ for the s -wave and $l = 1$ for the p -wave electrons. We have

$$S_0(p_e, p_\nu) = \frac{1}{3} p_\nu^2 \quad \text{and} \quad S_1(p_e, p_\nu) = \frac{1}{3} p_e^2 \frac{F_1(Z, E_e)}{F_0(Z, E_e)} . \quad (10)$$

The relativistic Fermi functions $F_0(Z, E_e)$ and $F_1(Z, E_e)$ account for the Coulomb interaction between the residual nucleus ($Z = 76$ in our case) and the emitted electron in the s and p -waves respectively. They are defined as

$$F_{k-1} = \left[\frac{\Gamma(2k+1)}{\Gamma(k)\Gamma(1+2\gamma_k)} \right]^2 (2p_e R)^{2(\gamma_k-k)} |\Gamma(\gamma_k + iz)|^2 e^{\pi z} \quad (11)$$

and depend on the strength of the Coulomb interaction, given by the fine structure constant $\alpha \simeq 1/137.03$, through

$$\gamma_k = \sqrt{k^2 - (\alpha Z)^2} \quad \text{and} \quad z = \alpha Z \frac{E_e}{p_e}, \quad (12)$$

$k = 1, 2$ in our case. We note that the Fermi functions in eq.(11) satisfy $F_{k-1}(Z \rightarrow 0, E_e) \rightarrow 1$ for $\alpha Z \rightarrow 0$ and for any $k \geq 1$.

The constant factor C , in eq. (8), is given by

$$C \equiv \frac{G_F^2 V_{ud}^2 c_V^2}{2\pi^3} \simeq 2 \times 10^{-36} (\text{keV})^{-4}, \quad (13)$$

where G_F is the Fermi constant, V_{ud} the element of the Cabibbo-Kobayashi-Maskawa matrix ($|V_{ud}| \simeq 0.97$), and $c_V \simeq 1$ is the vector strength of the charged weak interaction.

The dimensionless squared nuclear reduced matrix element (r. m. e.) B_{Re} is defined as

$$B_{Re} = \frac{g_A^2}{6R_{Re}^2} \left| \langle {}^{187}\text{Os}(1/2^-) \parallel \sum_{j=1}^{A=187} \tau_j^+ [\vec{\sigma}_j \otimes \vec{r}_j]_2 \parallel {}^{187}\text{Re}(5/2^+) \rangle \right|^2 \quad (14)$$

($6 = 2J + 1$ as $J = 5/2$) with $[\vec{\sigma}_j \otimes \vec{r}_j]_2$ a rank-2 tensor given by:

$$[\vec{\sigma} \otimes \vec{r}]_{2\mu} = \sum_{p,q=\pm 1,0} \langle 1p1q|2\mu \rangle \sigma_p r_q \quad (15)$$

where $\mu = \pm 2, \pm 1, 0$; $\vec{\sigma}_j, \vec{r}_j$ denote nucleon spin and space coordinates, respectively, and τ_j^+ is the isospin operator that transforms one neutron into one proton. The reduced matrix element can be computed directly from the experimental ${}^{187}\text{Re}$ mean-life $\tau = t_{1/2}/\ln 2$, [eq. (8)]

$$B_{Re}^{-1} = \tau C R_{Re}^2 \int_{m_e}^{E_0} p_e p_\nu E_e (E_0 - E_e) F_0(Z, E_e) S(p_e, p_\nu) dE_e, \quad (16)$$

and it takes the value $B_{Re} \simeq 3.6 \times 10^{-4}$ for a value of the nuclear radius R_{Re} approximated as $R_{Re} \simeq 1.2 \times (187)^{1/3} \text{fm} \simeq 6.86 \text{fm}$.

In Fig. 1 we represent on the left $d\Gamma_{s_{1/2}}^l/dE_e$ and $d\Gamma_{s_{1/2}}^s/dE_e$, and on the right $d\Gamma_{p_{3/2}}^l/dE_e$ and $d\Gamma_{p_{3/2}}^s/dE_e$; all these decay rates are normalized to one. We plot the sterile neutrino contribution, for s and p -waves outgoing single electron, for selected values of the sterile neutrino mass, $m_s = 1, 1.5$ and 2keV , compared to the light neutrino case with $m_l = 0$. Solid line corresponds to $m_l = 0$; and dashed, dash-dotted, dotted lines correspond to the sterile masses respectively.

In Fig. 2, we represent the non normalized decay rates: on the left $d\Gamma_{s_{1/2}}^l/dE_e$ and $d\Gamma_{s_{1/2}}^s/dE_e$, and on the right $d\Gamma_{p_{3/2}}^l/dE_e$ and $d\Gamma_{p_{3/2}}^s/dE_e$. Analogously to Fig. 1 the same neutrino masses are considered. As seen in the plots, the maximum differential decay rate for s -wave electrons is of the order of 10^7 , whereas for p -wave electrons it is 10^{11} . This dominance by four orders of magnitude of the p -wave is true for both light and sterile neutrino emission, and it has been noticed both theoretically [9] and experimentally [10]. This is why the spectral shape of beta decay is dictated by the curves shown in the r.h.s panel of Fig. 2.

The effect of the sterile neutrino emission on the electron spectral shape is qualitatively represented in Fig. 3 through the differential decay rate $d\Gamma/dE_e$ for $m_s = 1 \text{keV}$ and the dominant contribution $\cos^2 \zeta (d\Gamma^l/dE_e)$. To make the effect more dramatic a large unrealistic mixing angle $\sin^2 \zeta = 0.4$ is chosen. The two curves start to deviate at the *step* point $T_e = Q_\beta - m_s = 1.47 \text{keV}$, where the sterile neutrino starts to contribute, and the difference grows when T_e goes to zero.

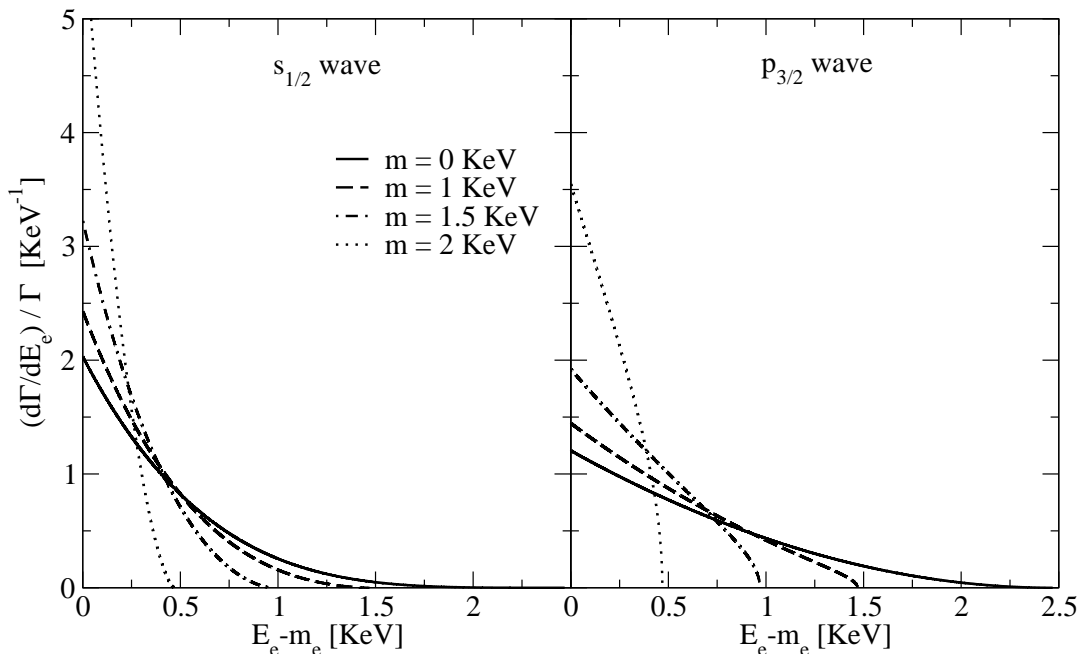


FIG. 1: Contributions of s -wave (left) and p -wave (right) electrons to the normalized differential decay rate of the process ^{187}Re to ^{187}Os against the electron kinetic energy $E_e - m_e$. Selected values of the sterile neutrino mass are used, $m_s = 1, 1.5, 2$ keV (dashed, dashed-dotted and dotted lines, respectively), compared to the light neutrino case $m_l = 0$ (solid line).

A. The ratio of the sterile neutrino to the active neutrino contribution and the Kurie plot

In order to analyze the possible effect of a sterile neutrino, we introduce the dimensionless function

$$\mathcal{R} \equiv \frac{d\Gamma^s/dE_e}{d\Gamma^l/dE_e} \tan^2 \zeta \quad (17)$$

that weights the relative contribution of the sterile neutrino to the light neutrino, times the tangent square of the mixing angle. The function \mathcal{R} is largest for p_e (or T_e) going to zero. This procedure is useful because we are comparing two regions of the same spectrum: the region where $(E_e - m_e) < (Q_\beta - m_s)$ and the emitted neutrino has enough energy such that the sterile neutrino ($m_s \sim \text{keV}$) imprints an effect on the spectrum, and the region where $(E_e - m_e) > (Q_\beta - m_s)$ and the sterile neutrino effect does not show up. Clearly, there is a *step* in the spectrum for $E_e - m_e = Q_\beta - m_s$ which could be observed if the experimental relative error in this energy region is lower than the height of the step.

The ratio \mathcal{R} [eq. (17)] is shown in Fig. 4 as a function of the electron momentum p_e for a fixed (unrealistic) mixing angle, $\zeta = 0.1^\circ$, and for different values of the neutrino masses: $m_s = 0, 1, 1.5$ and 2 keV, corresponding to the solid, dashed, dash-dotted and dotted lines respectively. As can be seen in this figure, the ratio is different from zero in the range $0 \leq p_e < (p_e)_{\text{max}}$, with $(p_e)_{\text{max}} = [(Q_\beta - m_s)(Q_\beta - m_s + 2m_e)]^{1/2}$. For example: for $m_s = 2$ keV, $(p_e)_{\text{max}} \simeq 21.7$ keV; and for $m_s = 1$ keV, $(p_e)_{\text{max}} \simeq 38.4$ keV. Notice that when m_s increases \mathcal{R} decreases.

Similarly, in Fig. 5 we show the ratio \mathcal{R} as a function of the electron momentum p_e but for a fixed sterile neutrino mass of $m_s = 1$ keV and different light-sterile mixing angles ζ : $\zeta = 0.1^\circ, 0.05^\circ, 0.01^\circ, 0.005^\circ$. Figure 5 shows not only the increase of \mathcal{R} with increasing mixing angle for a fixed value of m_s , but also shows the fact that for fixed values of m_s and ζ , the ratio \mathcal{R} is almost constant in the region $0 < p_e < (p_e)_{\text{max}}$.

From eq. (6) and eq. (7), we write

$$\frac{d\Gamma}{dE_e} = \frac{d\Gamma^l}{dE_e} [1 + \mathcal{R}] \cos^2 \zeta, \quad (18)$$

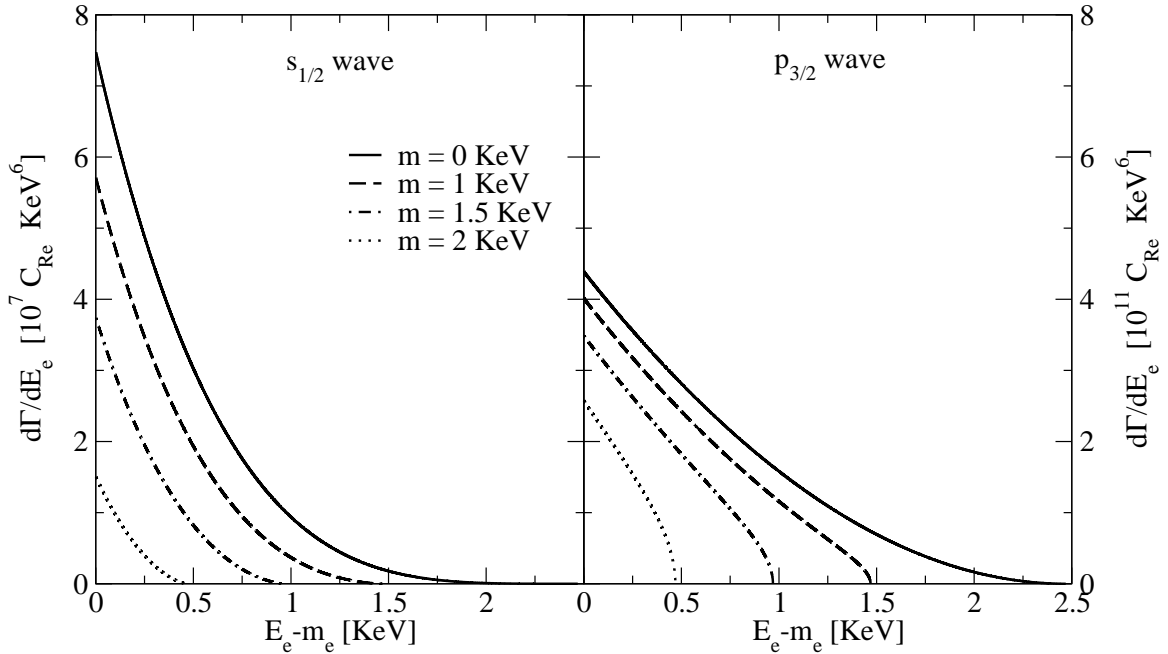


FIG. 2: Contributions of s-wave and p-wave electrons as in Fig. 1 of the process $^{187}\text{Re} \rightarrow ^{187}\text{Os}$ but for non-normalized decay rates in units of the constant $C_{Re} \equiv C B_{Re} R_{Re}^2$ in keV^6 . The maximum differential decay rate for s-wave electrons is of the order of 10^7 , whereas for p-wave electrons it is 10^{11} . The p-wave dominates by four orders of magnitude for both light and sterile neutrino emission and so the spectral shape of beta decay is dictated by the r.h.s. panel.

being $d\Gamma/dE_e$ the total differential decay rate where neutrino mixing is present ($\zeta \neq 0$), and $d\Gamma^l/dE_e$ the differential decay rate for the light neutrino (no mixing: $\zeta = 0$). For small mixing angle ζ , the differential decay rate $d\Gamma/dE_e$ [eq. (18)] normalized to $d\Gamma^l/dE_e$ is

$$\frac{d\Gamma/dE_e}{d\Gamma^l/dE_e} \simeq 1 + \mathcal{R}, \quad (19)$$

which shows that for small mixing angle the ratio between the differential decay rate [with mixing and without mixing] is given by $1 + \mathcal{R}$. This ratio will be largest for p_e or T_e going to zero.

We want to emphasize that the energy region suitable for creation and detection of the keV sterile (non relativistic) neutrino corresponds to low p_e or T_e . On the contrary, active neutrinos information should be obtained from the region of T_e close to the end-point energy Q_β .

From eqs. (6), (8) and (10), we can write for the function \mathcal{R} the explicit expression,

$$\mathcal{R} = \frac{p_{\nu_s}^3}{p_{\nu_l}^3} \theta(Q_\beta - T_e - m_s) \frac{1 + \frac{p_e^2}{p_{\nu_s}^2} \frac{F_1(Z, E_e)}{F_0(Z, E_e)}}{1 + \frac{p_e^2}{p_{\nu_l}^2} \frac{F_1(Z, E_e)}{F_0(Z, E_e)}} \tan^2 \zeta \quad (20)$$

In order to analyze the ratio $p_e^2 F_1(Z, E_e)/F_0(Z, E_e)$, it is worth to define $F_{k-1}(Z, E_e)$ as

$$F_{k-1}(Z, E_e) \equiv C_{k-1} d_{k-1} \left(\frac{m_e}{p_e} \right)^{2k-1} \left(\frac{E_e}{m_e} \alpha Z \right)^{2\gamma_{k-1}} \quad (21)$$

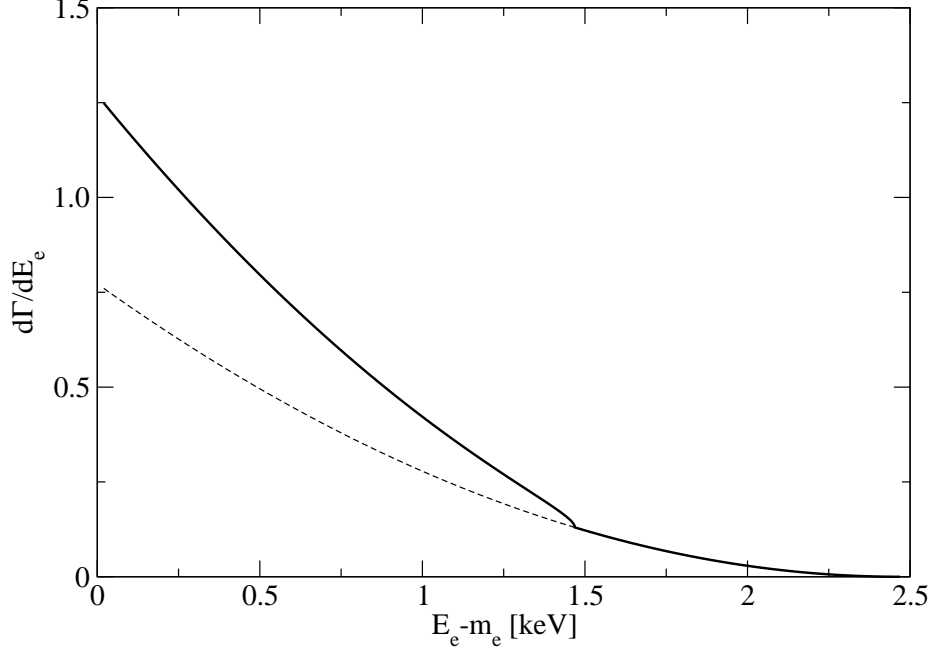


FIG. 3: Qualitative graph showing the differential decay rate of the process ^{187}Re to ^{187}Os vs. the electron kinetic energy considering light-sterile mixing for $m_s = 1$ keV and unrealistically large ζ (solid line) in order to visualize the sterile neutrino effect. The dashed line corresponding to $\cos^2 \zeta$ ($d\Gamma^l/dE_e$) without sterile component is shown for comparison.

where

$$C_{k-1} \equiv 2\pi(2m_e R)^{2(\gamma_k - k)} \left[\frac{\Gamma(2k+1)}{\Gamma(k)\Gamma(1+2\gamma_k)} \right]^2 \quad d_{k-1} \equiv \frac{1}{2\pi} \left(\frac{E_e}{p_e} \alpha Z \right)^{1-2\gamma_k} \left| \Gamma \left(\gamma_k + i \alpha Z \frac{E_e}{p_e} \right) \right|^2 e^{\pi \alpha Z \frac{E_e}{p_e}} \quad (22)$$

γ_k is defined by eq. (12) and $d_{k-1}(\alpha Z E_e/p_e) \rightarrow 1$ for $p_e \rightarrow 0$ (for all k). The above definitions yield again $F_{k-1} \rightarrow 1$ for $\alpha Z \rightarrow 0$ (for all k). In this respect, eqs. (21) and (22) differ from references [9] and [29, 30]. Finally, the ratio in the shape factor for $l = 1$ [eq.(10)] is given by

$$\frac{p_e^2 F_1(Z, E_e)}{F_0(Z, E_e)} = \frac{C_1}{C_0} \frac{d_1}{d_0} m_e^2 \left(\frac{E_e}{m_e} \alpha Z \right)^{2(\gamma_2 - \gamma_1)} \quad (23)$$

and for $p_e \rightarrow 0$

$$\frac{p_e^2 F_1(Z, E_e)}{F_0(Z, E_e)} \stackrel{p_e \rightarrow 0}{\sim} 0.4 m_e^2, \quad (24)$$

[$d_1/d_0 \rightarrow 1$ for $p_e \rightarrow 0$]. From eq. (20) and eq. (24), we have

$$\mathcal{R} \stackrel{p_e \rightarrow 0}{\sim} \frac{p_{\nu_s}}{p_{\nu_l}} \tan^2 \zeta. \quad (25)$$

For $p_e \rightarrow 0$, the maximum neutrino momenta are: $(p_{\nu_s})_{\max} \sim 1.45$ keV, 2.26 keV for $m_s \simeq 2$ keV, 1 keV respectively; and $(p_{\nu_l})_{\max} = 2.47$ keV for $m_l = 0$ keV [being $(p_e)_{\min} \simeq 0$].

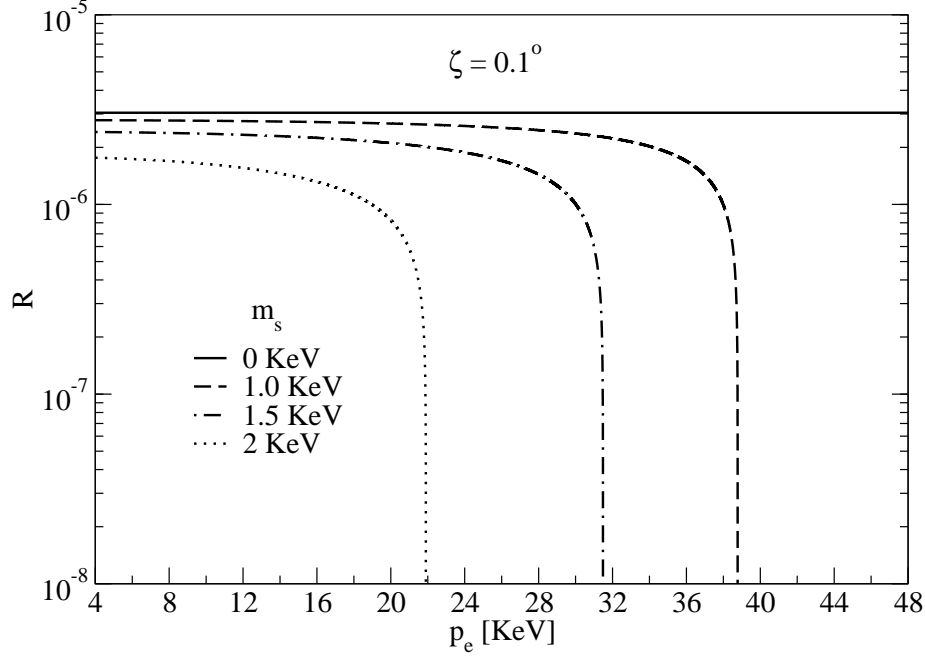


FIG. 4: Ratio \mathcal{R} [eq. (17)] of the sterile neutrino to the active neutrino contributions of the process ^{187}Re to ^{187}Os vs. the electron momentum for a fixed (unrealistic) mixing angle $\zeta = 0.1^\circ$ and different sterile neutrino masses, $m_s = 0, 1, 1.5$ and 2 keV (dashed, dashed-dotted and dotted lines, respectively). \mathcal{R} increases with decreasing m_s . \mathcal{R} is nonzero in a range $0 < p_e < p_{max}$ and p_{max} decreases as m_s increases.

We have shown the relevance of the function \mathcal{R} in order to analyze the effect of a sterile neutrino. One can also study the effect of a sterile neutrino through the difference between the decay rate with mixing ($\zeta \neq 0$) and the reference case without mixing ($\zeta = 0$). This difference is very small, since the mixing is in any case small, as it is expressed in the following ratio:

$$\mathcal{R}^* = \frac{\left[\frac{d\Gamma}{dE_e} \right]_{\zeta \neq 0} - \left[\frac{d\Gamma}{dE_e} \right]_{\zeta = 0}}{\left[\frac{d\Gamma}{dE_e} \right]_{\zeta = 0}} = \left(-1 + \frac{d\Gamma^s/dE_e}{d\Gamma^l/dE_e} \right) \sin^2 \zeta = \frac{d\Gamma/dE_e}{d\Gamma^l/dE_e} - 1, \quad (26)$$

which can be written as well as a function of \mathcal{R}

$$\mathcal{R}^* = -\sin^2 \zeta + \mathcal{R} \cos^2 \zeta \quad (27)$$

In Fig. 6 we plot the quantity \mathcal{R}^* for a fixed sterile mass $m_s = 1$ keV and for different mixing angles.

The Kurie function is defined as

$$K(y) = \sqrt{\frac{d\Gamma/dE_e}{p_e E_e F_0(Z, E_e)}} \quad , \quad y \equiv E_o - E_e = Q - T_e \geq 0 \quad (28)$$

Considering the mixing between the light and sterile neutrinos, $K(y)$ can be written as

$$K(y) = \sqrt{K_l^2(y) \cos^2 \zeta + K_s^2(y) \sin^2 \zeta} \quad (29)$$

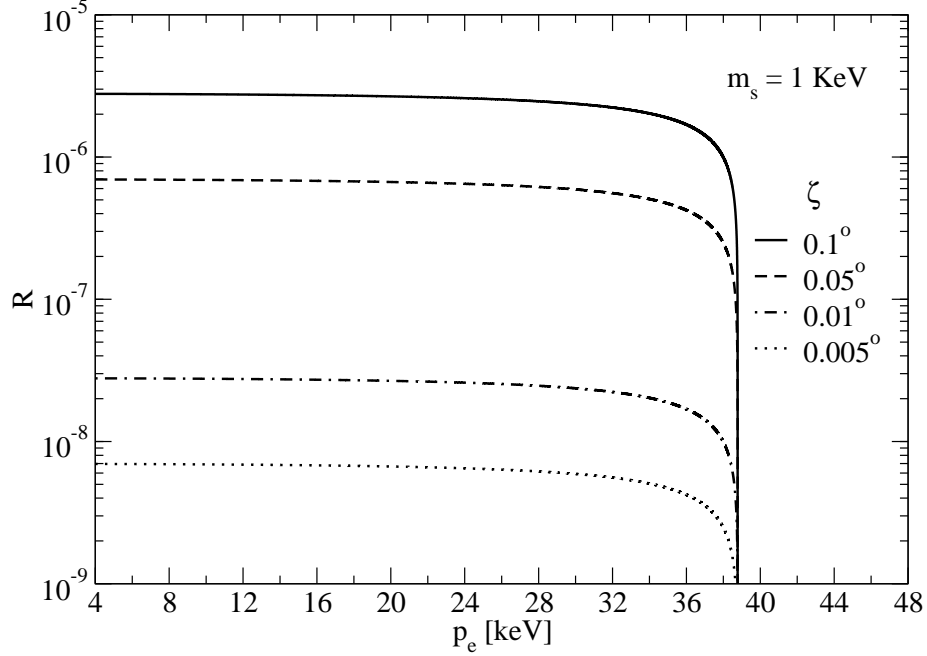


FIG. 5: The ratio \mathcal{R} as in Fig. 4 but for a fixed sterile neutrino mass $m_s = 1$ keV and different mixing angles, $\zeta = 0.1^\circ, 0.05^\circ, 0.01^\circ, 0.005^\circ$ (solid, dashed, dashed-dotted and dotted lines, respectively) of the process ^{187}Re to ^{187}Os . \mathcal{R} is almost constant in the range $0 < p_e < p_{max}$ and increases with ζ .

where

$$K_\chi(y) = \sqrt{\frac{d\Gamma^\chi/dE_e}{p_e E_e F_0(Z, E_e)}} \quad , \quad \chi = l, s \quad . \quad (30)$$

For $\zeta = 0$ (no sterile-light neutrino mixing), and due to the introduction of $F_0(Z, E_e)$ in the denominator, $K(y)$ vs. y is a straight line for $m_l \simeq 0$. $K(y)$ can be written as well in terms of \mathcal{R} eq. (17),

$$K(y) = K_l \sqrt{1 + \mathcal{R}} \cos \zeta \quad . \quad (31)$$

Finally, in Fig. 7 we present the Kurie plot for K_s considering several sterile neutrino masses m_s , and K_l (solid line).

V. THE STERILE NEUTRINO MASS AND THE TRITIUM BETA DECAY

Let us now consider the beta decay of Tritium ^3H ($Z = 1$; $A = 3$)



as a probe to detect a possible mixing of keV sterile neutrinos with active neutrinos. ^3H is a hydrogen isotope going to the helium isotope ^3He , with a half-life $t_{1/2} \simeq 12.33$ years, end-point energy $Q_\beta \simeq 18.59$ keV, and a spin-parity transition $1/2^+ \rightarrow 1/2^+$.

For the Tritium decay case ^3H , there is no change in angular momentum and parity corresponding to an allowed transition ($L = 0$) with Fermi ($S = 0$) and Gamow-Teller ($S = 1$) components. Therefore, the single electron is emitted in s -wave and the differential decay rate is simply

$$\frac{d\Gamma}{dE_e} = \frac{d\Gamma_{s_{1/2}}}{dE_e} \quad (33)$$

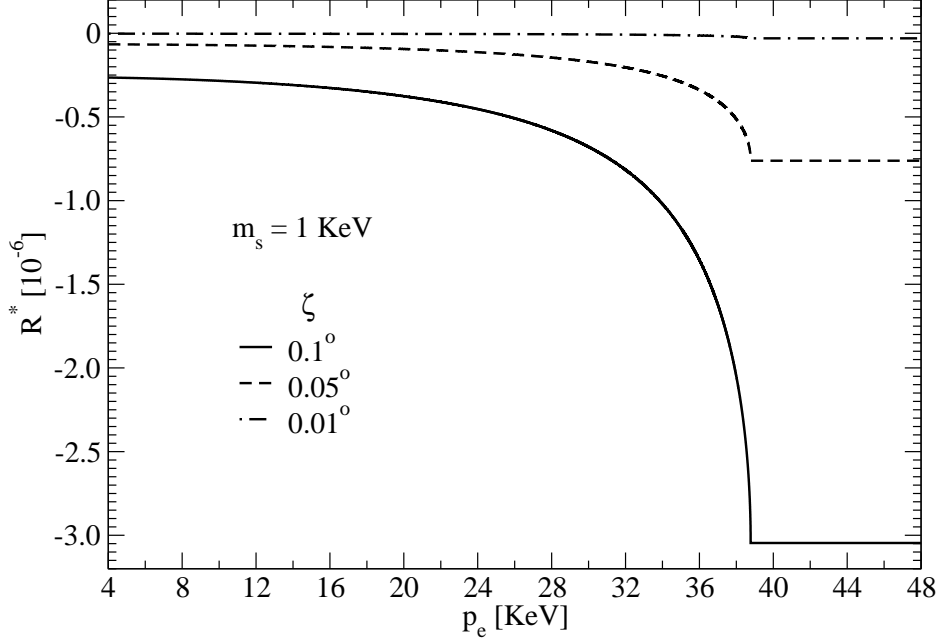


FIG. 6: Same as in Fig. 5 but for \mathcal{R}^* [eq. (26) or eq. (27)] in units of 10^{-6} for fixed m_s and different mixing angles of the process ^{187}Re to ^{187}Os . The small p_e region is always the best for the sterile neutrino detection.

Similarly to eq. (7) and eq. (8) we have

$$\frac{d\Gamma_{s_{1/2}}}{dE_e} = \frac{d\Gamma_{s_{1/2}}^l}{dE_e} \cos^2 \zeta + \frac{d\Gamma_{s_{1/2}}^s}{dE_e} \sin^2 \zeta \quad (34)$$

and

$$\frac{d\Gamma_{s_{1/2}}^\chi}{dE_e} = C B_T p_e p_{\nu_\chi} E_e (E_0 - E_e) F_0(Z, E_e) \theta(E_0 - E_e - m_\chi) \quad , \quad \chi = l, s \quad , \quad (35)$$

as the shape factor $S(p_e, p_\nu) = 1$ for allowed decays. Here, the squared reduced matrix element (r.m.e) for the allowed decay of Tritium ^3H (T), will be

$$B_T = B_F + B_{GT} \quad (36)$$

where B_F and B_{GT} are the Fermi and Gamow-Teller decay strengths given by:

$$B_F = \frac{1}{2} |\langle ^3\text{He}(1/2^+) \| \sum_{j=1}^{A=3} \tau_j^+ \| ^3\text{H}(1/2^+) \rangle|^2 \quad (37)$$

and

$$B_{GT} = \frac{g_A^2}{2} |\langle ^3\text{He}(1/2^+) \| \sum_{j=1}^{A=3} \tau_j^+ \vec{\sigma}_j \| ^3\text{H}(1/2^+) \rangle|^2 \quad (38)$$

where $g_A = c_A/c_V \simeq 1.26$ is the axial-to-vector strength ratio of the charged weak interaction. From the experimental half-life of Tritium one obtains a value of the squared r.m.e. $B_T \simeq 5.61$.

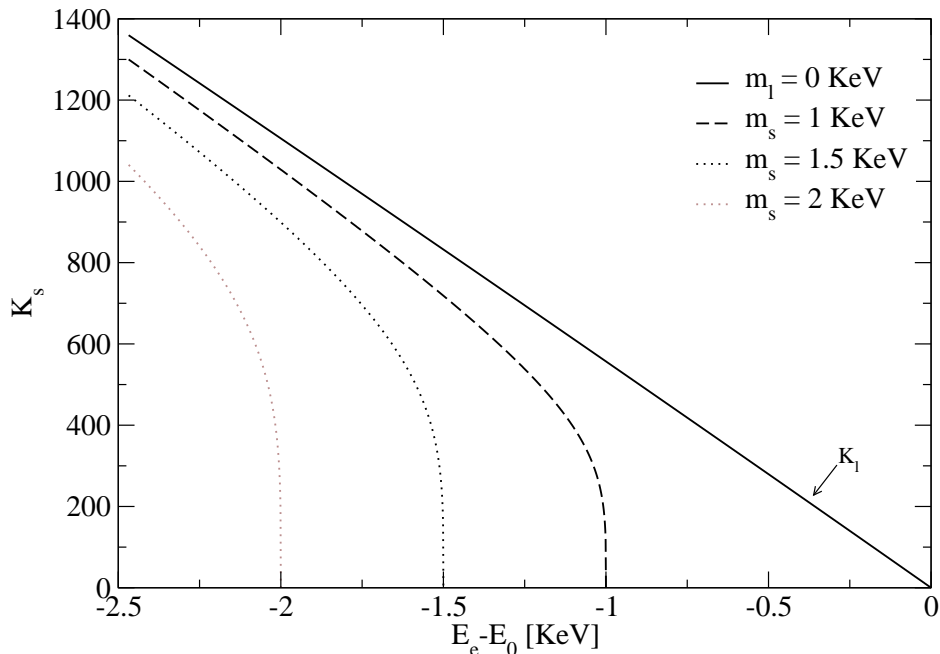


FIG. 7: Kurie plot K_s of the process ^{187}Re to ^{187}Os for sterile neutrino masses of $m_s = 1, 1.5$ and 2 keV as well as K_l for a light neutrino mass $m_l = 0$.

In Fig. 8 we plot the differential decay rates of the process ^3H to ^3He , normalized to 1. We consider the emission of a light neutrino, $m_l = 0$ (solid line); and a sterile neutrino with masses $m_s = 1, 1.5$ and 2 keV (dashed, dashed-dotted and dotted lines respectively).

In Fig. 9 we plot the ratio \mathcal{R} vs. p_e for a fixed sterile neutrino mass ($m_s = 1$ keV) and different mixing angles.

VI. CONCLUSIONS

The detection of sterile neutrinos is not only important from the point of view of particle physics for the extension of the SM, but also from the point of view of cosmology and astrophysics as a serious candidate for dark matter in the keV mass range. With the relevance of the search and detection of keV scale dark matter candidates in mind, we have studied Rhenium 187 and Tritium beta decays. The low electron energy domain of the beta spectrum is the region where a sterile neutrino could be detected and its mass measured, the expected mass being in the keV scale (1 to 10 keV) as constrained from cosmological and galactic observations and theoretical analysis. The electron low energy region suitable to detect the sterile neutrino, $0 \text{ keV} \lesssim T_e \lesssim (Q_\beta - m_s) \text{ keV}$, is away from the near end-point energy range suitable for the detection of the active neutrino mass.

Two very important experiments are running at present: MARE and KATRIN dealing with Rhenium 187 and Tritium beta decays respectively. The MARE experiment will provide the entire shape of the electron differential decay rate, giving data for both the sterile and the active neutrino detection regions. KATRIN so far concentrates on the region near the end-point of the electron spectrum but it would be extremely interesting to also look for data for the sterile neutrino in the mass keV region. In this paper, we have carried out the study for the detection of a sterile neutrino in the expected keV mass range considering different mixing angles, according to astronomical and cosmological observations and experiments.

In order to detect the small relative deviation in the experimental spectrum due to the sterile neutrino mixing, the experimental relative error (inversely proportional to the square root of the number of measured events, $\epsilon \sim N_\beta^{-1/2}$)

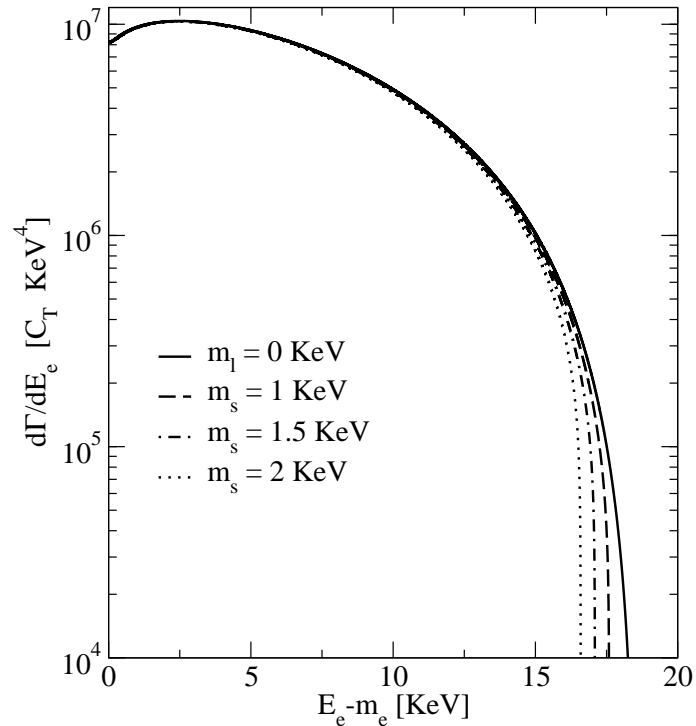


FIG. 8: Differential decay rate for the Tritium process ${}^3\text{H}$ going to ${}^3\text{He}$ with the emission of active ($m_l = 0$) or sterile ($m_s = 1, 1.5, 2$ keV) neutrinos, in units of the constant $C_T \equiv C B_T$ in keV^4 ; the vertical axis is in logarithmic scale.

must be as small as possible. In order to reduce the experimental relative error, the number of detected events must be increased, for instance by choosing a beta decay with a small Q_β value, as it is the case of the Rhenium, and by increasing the time of data acquisition. For MARE, the typical number of events is $10^{13} - 10^{14}$, (for 10 years of data acquisition, 8 arrays and 400 gr of natural Rhenium [7]). We found that the largest ratio \mathcal{R} for a realistic mixing angle is about 10^{-8} , [dotted line and small p_e region in our Fig. 5], therefore the sterile neutrino probability $\mathcal{R} \times N_\beta$ is about $10^5 - 10^6$, which is not negligible. That means to find such $10^5 - 10^6$ sterile neutrinos in those $10^{13} - 10^{14}$ events. This figure is increased in an order of magnitude for the MARE option of 10^{15} events, [for 10 years of data acquisition, 16 arrays and 3.2 kg. of natural Rhenium, [7]]. Of course, in order to assess a precise prediction of the detection probability one should include a careful analysis of the systematics errors and instrument parameters, but such study is beyond the scope of the present paper.

Acknowledgments

We are grateful to Peter Biermann, Angelo Nucciotti and Christian Weinheimer for useful discussions. O.M and E.M.G acknowledge the financial support of the Spanish Ministry of Science and Education (FIS 2008-01301, FIS 2011-23565 and FPA 2010-17142). M.R.M. acknowledges the financial support of the Spanish Ministry of Science and Education (FIS 2008-01323), and the kind hospitality of the Observatoire de Paris.

-
- [1] J. R. Bond, A. S. Szalay, *Astrophys. J.* **274**, 443 (1983). J R Bond, A S Szalay, M S Turner, *Phys. Rev. Lett.* **48**, 1636 (1982).
 [2] C. J. Hogan, J. J. Dalcanton, *Phys. Rev.* **D62**, 063511 (2000). J. J. Dalcanton, C. J. Hogan, *Astrophys. J.* **561**, 35 (2001). S. Dodelson, L. M. Widrow, *Phys. Rev. Lett.* **72**, 17 (1994). X. Shi, G. M. Fuller, *Phys. Rev. Lett.* **82**, 2832 (1999). K. Abazajian, G. M. Fuller, M. Patel, *Phys. Rev.* **D64**, 023501 (2001); K. Abazajian, G. M. Fuller, *Phys. Rev.* **D66**, 023526,

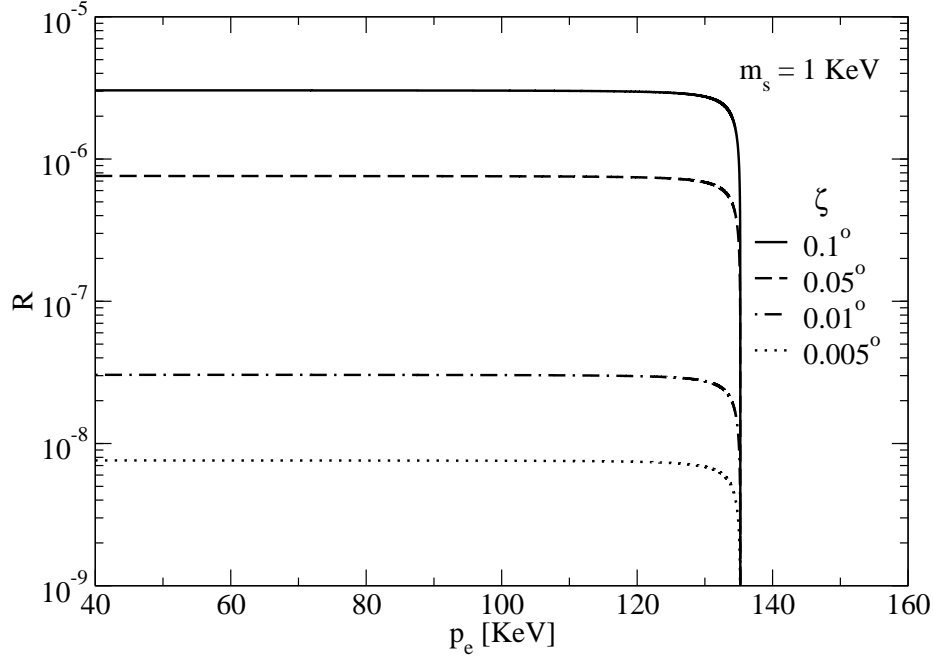


FIG. 9: Ratio \mathcal{R} [eq. (17)] vs. the electron momentum for a fixed sterile neutrino mass $m_s = 1$ keV and different mixing angles, for the process ${}^3\text{H}$ going to ${}^3\text{He}$.

- (2002); G. M. Fuller *et al.*, Phys. Rev. **D68**, 103002 (2003); K. Abazajian, Phys. Rev. **D73**, 063506 (2006). P. L. Biermann, A. Kusenko, Phys. Rev. Lett. **96**, 091301 (2006); T. Asaka, M. Shaposhnikov, A. Kusenko; Phys. Lett. **B638**, 401 (2006).
- [3] H.J. de Vega and N. Sánchez, Mon. Not. R. Astron. Soc. **404**, 885 (2010), astro-ph/0901.0922. D. Boyanovsky, H.J. de Vega and N. Sánchez, Phys Rev **D77**, 043518 (2008).
- [4] H.J. de Vega and N. Sánchez Int. J. Mod. Phys. **A 26**, 1057 (2011). H.J. de Vega, P. Salucci and N. Sánchez, astro-ph/1004.1908.
- [5] A. D. Dolgov, Phys. Rept. 370 (2002) 333-535. F. Munyaneza, P. L. Biermann, Astron. and Astrophys., 458, L9 (2006). A. Kusenko, Phys. Rept. 481, 1 (2009). D. Boyanovsky, C. M. Ho, JHEP, 0707 (2007).
- [6] F. D. Steffen, Eur. Phys. J. C59, 557 (2009).
- [7] MARE collaboration, <http://mare.dfm.uninsubria.it/frontend/exec.php>; A. Nucciotti, Neutrino 2010, arXiv:1012.2290. A. Nucciotti, on behalf of the MARE collaboration, "The MARE experiment and its capabilities to measure the light (active) and heavy (sterile) neutrinos", lecture at the Chalonge Meudon Workshop 2011: Warm Dark Matter in the Galaxies, Theory and Observations, available at <http://chalonge.obspm.fr/>
- [8] M. Galeazzi *et al.* PRL, 86, 1978 (2001).
- [9] R. Dvornický, K. Muto, F. Šimkovic and A. Faessler, Phys. Rev. **C83**, 045502 (2011).
- [10] C. Arnaboldi *et al.*, Phys. Rev. Lett. **96**, 042503 (2006).
- [11] KATRIN collaboration, <http://www-ik.fzk.de/tritium/>; C. Weinheimer, Varenna Enrico Fermi Course CLXX, arXiv:0912.1619. C. Weinheimer, "Absolute Scale of the Neutrino Mass and the Search for Neutrinoless Double Beta Decay", lecture at the 15th Paris Cosmology Colloquium 2011: From CDM to WDM in the Standard Model of the Universe: Theory and Observations, available at <http://chalonge.obspm.fr/>
- [12] F. Zwicky, Helv. Phys. Acta, 6, 124 (1933).
- [13] J. H. Oort, ApJ, 91, 273 (1940). See S. van den Bergh, astro-ph/0005314 for a history of the research on dark matter.
- [14] E. W. Kolb, M. S. Turner, *The Early Universe*, Addison-Wesley (1990).
- [15] D. Boyanovsky, H.J. de Vega and N. Sánchez, Phys Rev **D78**, 063546 (2008).
- [16] S. Dodelson, *Modern Cosmology*, Academic Press, London, (2003).
- [17] J Kormendy, K C Freeman, IAU Symposium, Sydney, 220, 377 (2004), arXiv:astro-ph/0407321. M. Spano *et al.*, MNRAS, 383, 297 (2008). G. Gentile *et al.*, Nature, 461, 627 (2009). F. Donato *et al.*, MNRAS **397**, 1169 (2009).
- [18] Y. Hoffman *et al.*, Astrophysical Journal 671, 1108 (2007).
- [19] J. Zavala *et al.* Ap. J, 700, 1779 (2009). E. Papastergis, *et al.* arXiv:1106.0710, to appear in ApJ.

- [20] R. E. Smith, K. Markovic, arXiv:1103.2134. K. Markovic et al. JCAP 1101:022 (2011).
- [21] A. Kamada, N. Yoshida, 'keV-mass sterile neutrino dark matter and the structure of galactic halos', lecture at the 15th Paris Cosmology Colloquium 2011: From CDM to WDM in the Standard Model of the Universe: Theory and Observations, available at <http://chalonge.obspm.fr/>
- [22] H.J. de Vega and N. Sánchez *Highlights and Conclusions of the Chalonge Meudon Workshop Dark Matter in the Universe*, astro-ph/1007.2411
- [23] H.J. de Vega, M.C. Falvella and N. Sánchez *Highlights and Conclusions of the Chalonge 14th Paris Colloquium: The Standard Model of the Universe: Theory and Observations*, astro-ph/1009.3494.
- [24] V. Tikhonov, S. Gottloeber, G. Yepes and Y. Hoffman, MNRAS 399, 1611 (2009).
- [25] M. Loewenstein, A. Kusenko, P. L. Biermann, *Astrophys. J.* **700**, 426 (2009). M. Loewenstein, A. Kusenko, *Astrophys. J.* **714**, 652 (2010).
- [26] G. G. Raffelt and Shun Zhou, *Phys. Rev. D* 83, 093014 (2011).
- [27] M. Viel et al. *Phys. Rev. D*, vol. 71 pp. 63534, (2005).
- [28] A. Boyarsky, O. Ruchayskiy, M. Shaposhnikov, *Ann. Rev. Nucl. Part. Sci.* 59, 191 (2009). A. Boyarsky, J. Lesgourgues, O. Ruchayskiy, M. Viel, *Phys. Rev. Lett.* 102, 201304 (2009).
- [29] M. Doi, T. Kotani and E. Takasugi *Prog. Theor. Phys. (Supp.)* **83**, 1 (1985).
- [30] M. Doi and T. Kotani *Prog. Theor. Phys.* **87**, 1207 (1992).
- [31] Y. Chikashige, R. N. Mohapatra, R. D. Peccei, *Phys. Lett.* 98B, 265 (1981). J. Schechter, J.W.F. Valle, *Phys. Rev. D* 25, 774 (1982). R. R. Volkas, *Prog. Part. Nucl. Phys.* 48, 161 (2002). M. Shaposhnikov, I. Tkachev, *Phys. Lett.* B639, 414 (2006). F. Bezrukov, H. Hettmansperger, M. Lindner, *Phys.Rev. D* 81: 085032 (2010). M. Lindner, A. Merle, and V. Niro, JCAP **1101** (2011) 034. A. Merle and V. Niro, JCAP 07 (2011) 023.
- [32] H. Behrens and W. Bühring. *Electron radial wave functions and nuclear beta decay*. Clarendon Press Oxford 1982.